Supplementary Information for

Pronounced spatial disparity of projected heatwave changes in the Northern Hemisphere linked to heat domes and soil moisture-temperature coupling

Fenying Cai [1, 2], Caihong Liu [3], Dieter Gerten [1, 2], Song Yang [4, 5], Tuantuan Zhang [4, 5]*, Shuheng Lin [4], and Jürgen Kurths [1, 6]

[1] Potsdam Institute for Climate Impact Research (PIK), Member of the Leibniz Association, 14473 Potsdam, Germany

[2] Department of Geography, Humboldt-Universität zu Berlin, 10099 Berlin, Germany

[3] Department of Water and Climate Risk, Institute for Environmental Studies, Vrije University Amsterdam, 1087HV Amsterdam, Netherlands

[4] School of Atmospheric Sciences, Sun Yat-sen University, and Southern Marine Science and Engineering Guangdong Laboratory (Zhuhai), 519082 Zhuhai, China

[5] Guangdong Province Key Laboratory for Climate Change and Natural Disaster Studies, Sun Yat-sen University, 519082 Zhuhai, China

[6] Department of Physics, Humboldt-Universität zu Berlin, 10099 Berlin, Germany

*Corresponding authors: Tuantuan Zhang (zhangtt75@mail.sysu.edu.cn)

Table S1 | List of 14 CMIP6 models.

Model	Institution
ACCESS-CM2	Alfred Wegener Institute, Helmholtz Centre for Polar and Marine Research (AWI), Germany
CanESM5	Canadian Centre for Climate Modelling and Analysis, Environment and Climate Change Canada, Canada
EC-Earth3	EC-Earth consortium, Rossby Center, Swedish Meteorological and Hydrological Institute/SMHI, Norrkoping, Sweden
GFDL-CM4	National Oceanic and Atmospheric Administration, Geophysical Fluid Dynamics Laboratory, Princeton, NJ, USA
INM-CM5-0	Institute for Numerical Mathematics (INM), Russian Academy of Science, Moscow, Russia
IPSL-CM6A-LR	Institute Pierre Simon Laplace (IPSL), Paris, France
KACE-1-0-G	National Institute of Meteorological Sciences/Korea Meteorological Administration, Climate Research Division, Korea
MIROC6	Japan Agency for Marine-Earth Science and Technology (JAMSTEC), Atmosphere and Ocean Research Institute (AORI), The University of Tokyo, National Institute for

	Environmental Studies (NIES), and RIKEN Center for Computational Science, Japan
MPI-ESM1-2-HR	Max Planck Institute for Meteorology (MPI-M), Germany
MPI-ESM1-2-LR	Max Planck Institute for Meteorology (MPI-M), Germany
MRI-ESM2-0	Meteorological Research Institute (MRI), Japan
NorESM2-LM	NorESM Climate Modeling Consortium, Norway
NorESM2-MM	NorESM Climate Modeling Consortium, Norway
UKESM1-0-LL	Met Office Hadley Centre, Exeter, UK

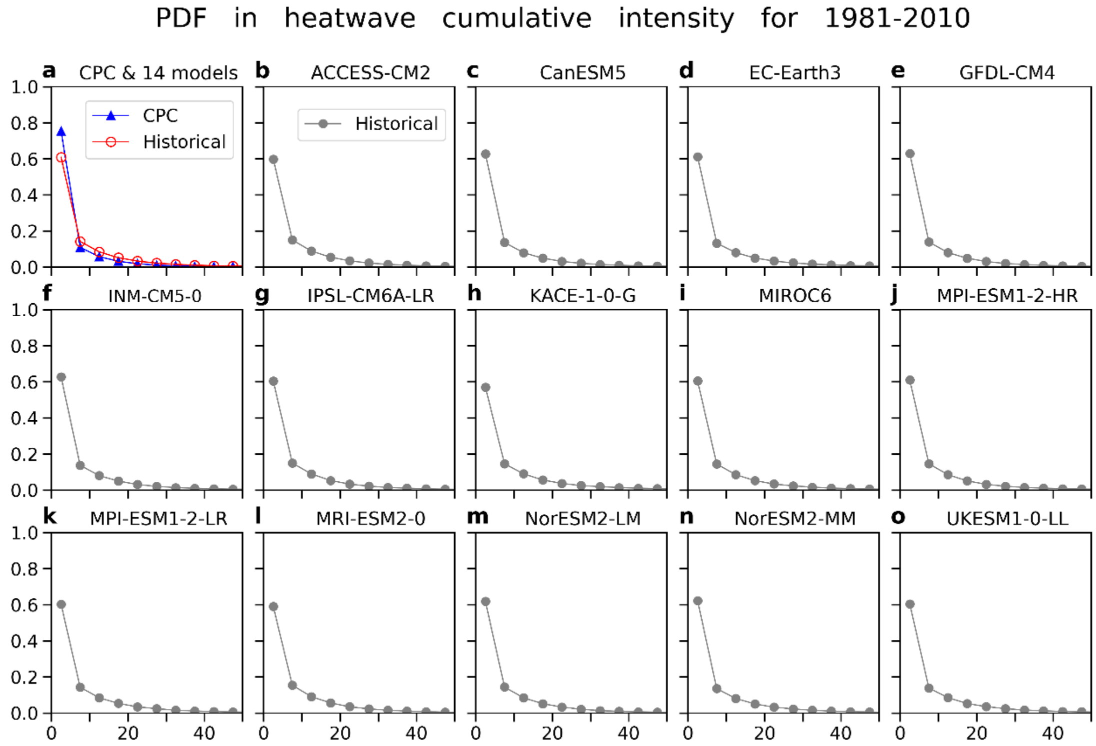

Figure S1. Observed and simulated probability density function (PDF) in heatwave cumulative intensity. Simulated PDF in heatwave cumulative intensity (HWI; units: K) during 1981–2010 in historical simulation by **(a)** all 14 models (red line with hollow circles), and by **(b)** ACCESS-CM2 (gray line with solid circles), **(c)** CanESM5, **(d)** EC-Earth3, **(e)** GFDL-CM4, **(f)** HadGEM3-GC31-LL, **(g)** INM-CM5-0, **(h)** IPSL-CM6A-LR, **(i)** MIROC6, **(j)** MPI-ESM1-2-HR, **(k)** MPI-ESM1-2-LR, **(l)** MRI-ESM2-0, **(m)** NorESM2-LM, **(n)** NorESM2-MM, and **(o)** UKESM1-0-LL. Observed PDF in HWI during the period 1981–2010 in CPC dataset (blue line with triangles) is also shown in **(a)**.

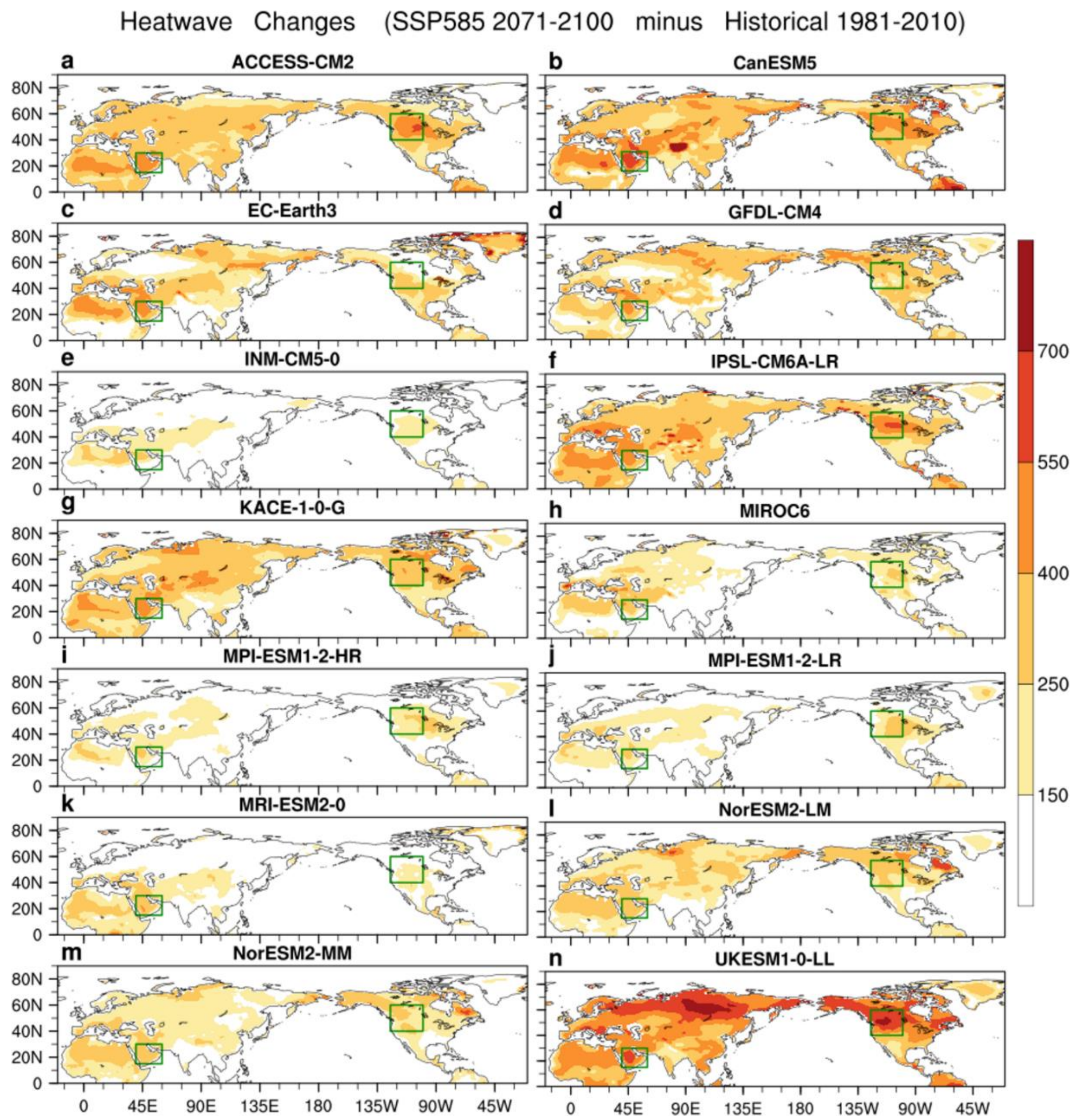

Figure S2. Long-term future projected changes in HWI under the SSP585 scenario by 14 CMIP6 models. Future change is calculated as the averaged difference between 2071–2100 under the SSP585 scenario and 1981–2010 in historical simulation for HWI (units: K) by models **(a)** ACCESS-CM2, **(b)** CanESM5, **(c)** EC-Earth3, **(d)** GFDL-CM4, **(e)** HadGEM3-GC31-LL, **(f)** INM-CM5-0, **(g)** IPSL-CM6A-LR, **(h)** MIROC6, **(i)** MPI-ESM1-2-HR, **(j)** MPI-ESM1-2-LR, **(k)** MRI-ESM2-0, **(l)** NorESM2-LM, **(m)** NorESM2-MM, and **(n)** UKESM1-0-LL. Green boxes in **(a–n)** present the domain of western Asia (15°–30°N, 40°–60°E) and western North America (40°–60°N, 125°–100°W).

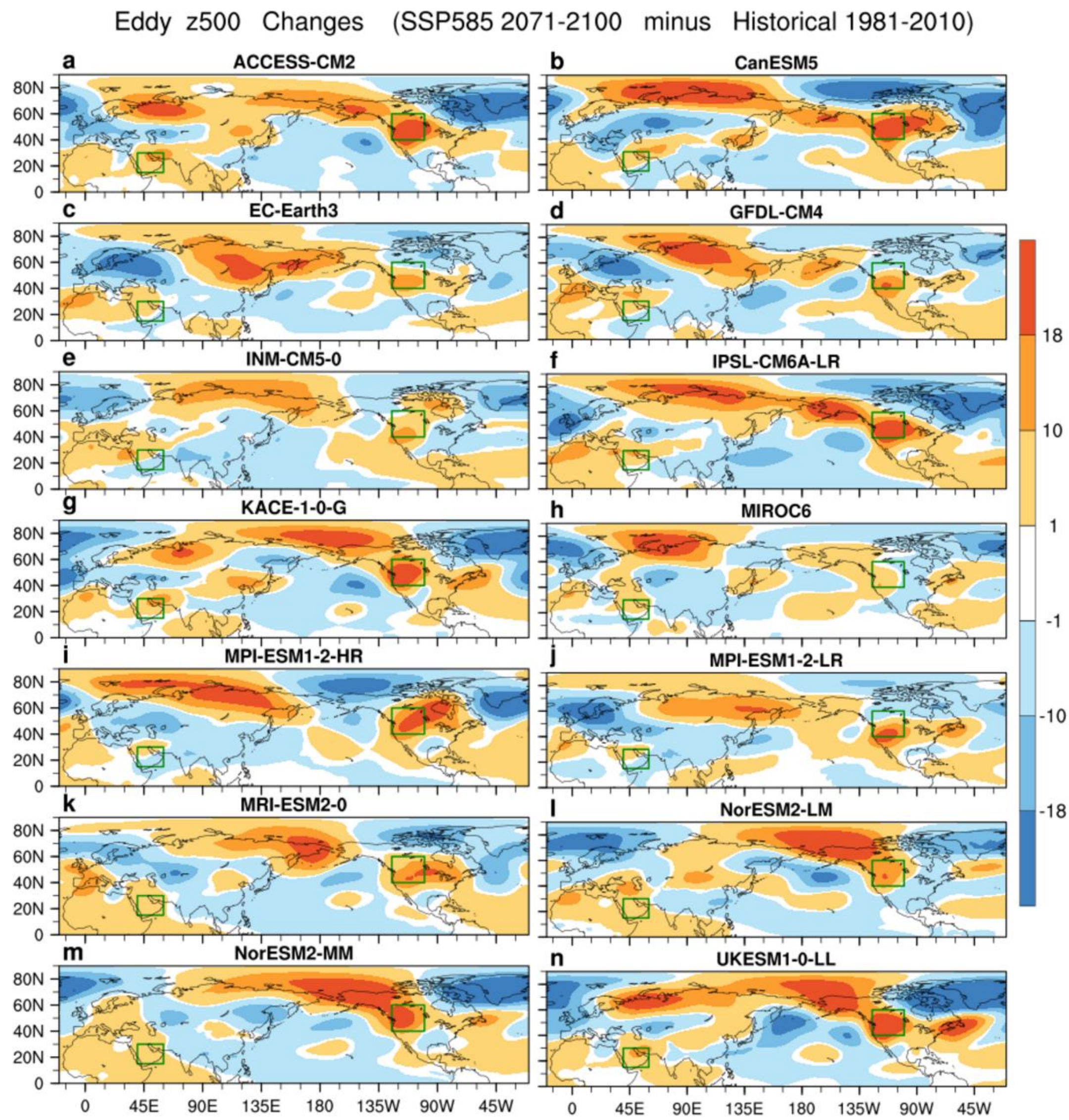

Figure S3. Long-term future projected changes in eddy z500 under the SSP585 scenario by 14 CMIP6 models. Future change is calculated as the averaged difference between 2071–2100 under the SSP585 scenario and 1981–2010 in historical simulation for eddy z500 (units: gpm) by models **(a)** ACCESS-CM2, **(b)** CanESM5, **(c)** EC-Earth3, **(d)** GFDL-CM4, **(e)** HadGEM3-GC31-LL, **(f)** INM-CM5-0, **(g)** IPSL-CM6A-LR, **(h)** MIROC6, **(i)** MPI-ESM1-2-HR, **(j)** MPI-ESM1-2-LR, **(k)** MRI-ESM2-0, **(l)** NorESM2-LM, **(m)** NorESM2-MM, and **(n)** UKESM1-0-LL. Green boxes in **(a–n)** present the domain of western Asia (15°–30°N, 40°–60°E) and western North America (40°–60°N, 125°–100°W).

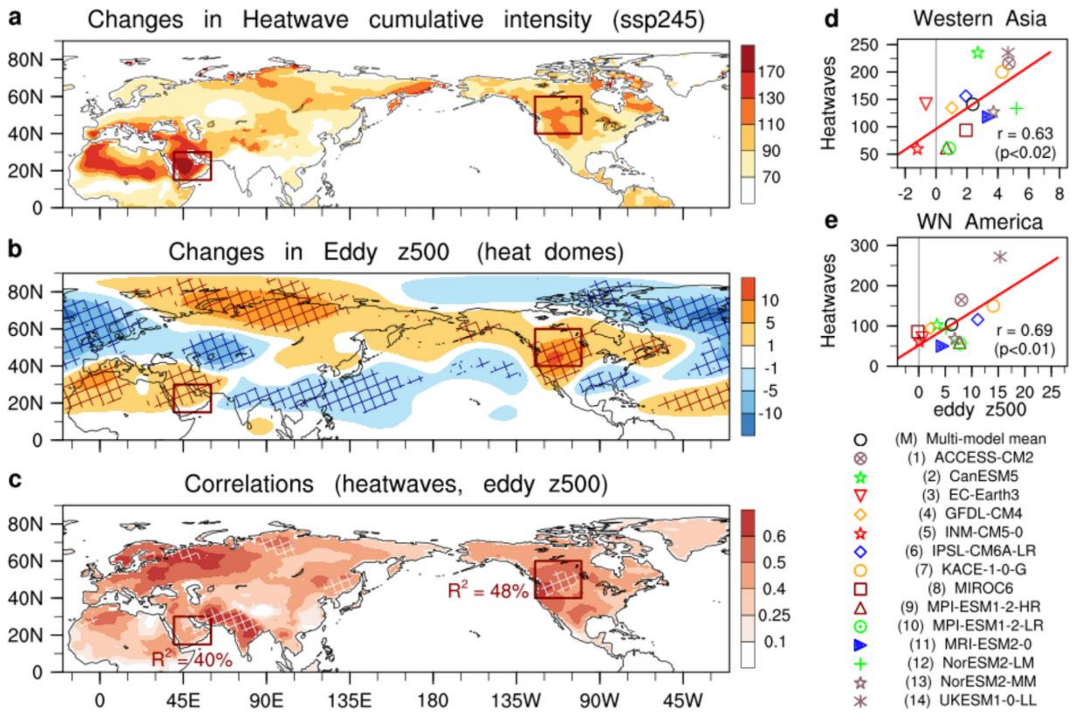

Figure S4. Multi-model mean of long-term future summertime heatwave and eddy z500 changes in the Northern Hemisphere under the future SSP245 scenario. Future change is calculated as the averaged difference between 2071–2100 under the SSP245 scenario and 1981–2010 in historical simulation for **(a)** HWI (units: K) and **(b)** eddy z500 (units: gpm). Hatched areas in **(b)** show where at least 10 models (> 78% of the total 14 models) simulate the eddy z500 changes with same signs. **(c)** Correlation between projected heatwave cumulative intensity and eddy z500 in 420 summers during the 2071–2100 under the SSP585 scenario by 14 models. Simulated heatwave cumulative intensity changes (units: K) versus eddy z500 changes (units: gpm) for **(d)** western Asia and **(e)** western North America. The red boxes in **(a–c)** present the domain of western Asia and western North America. The explained variances (R^2) between heatwave changes and eddy z500 changes for western Asia and western North America are also shown in **(c)**. The labels denoting the 14 models are shown in the bottom right corner.

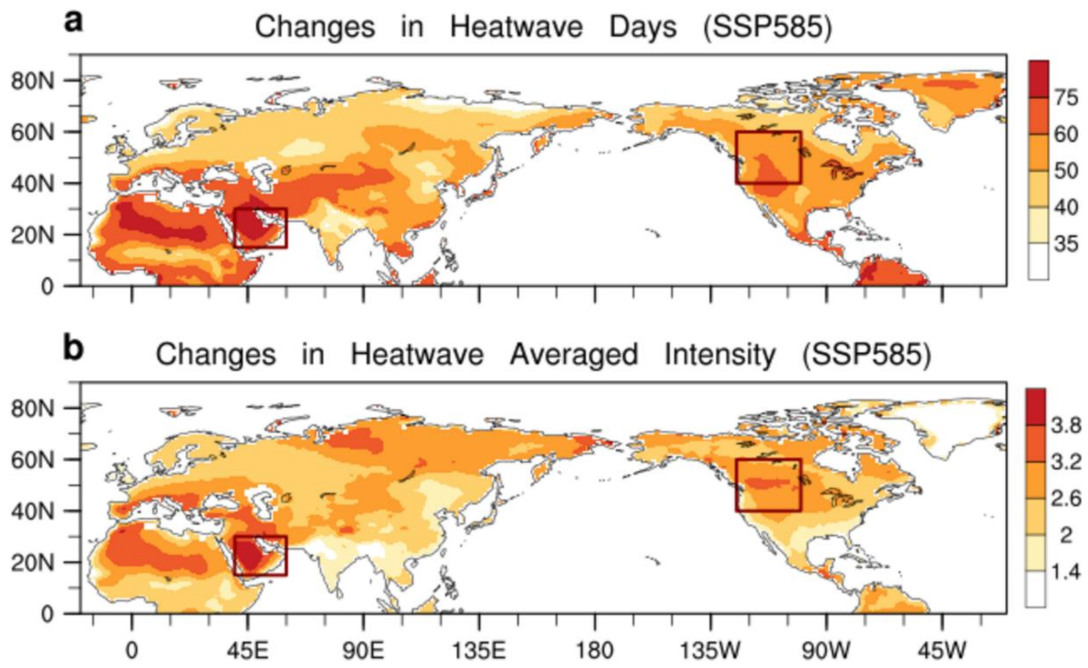

Figure S5. Multi-model mean of long-term future summertime heatwave changes in the Northern Hemisphere under the future SSP585 scenario. Averaged difference between 2071–2100 under the SSP585 scenario and 1981–2010 in historical simulation from 14 CMIP6 models for **(a)** number of heatwave cumulative days (units: day) and **(b)** heatwave averaged intensity (units: K). The red boxes in **(a–b)** present the domain of western Asia (15°–30°N, 40°–60°E) and western North America (40°–60°N, 125°–100°W).

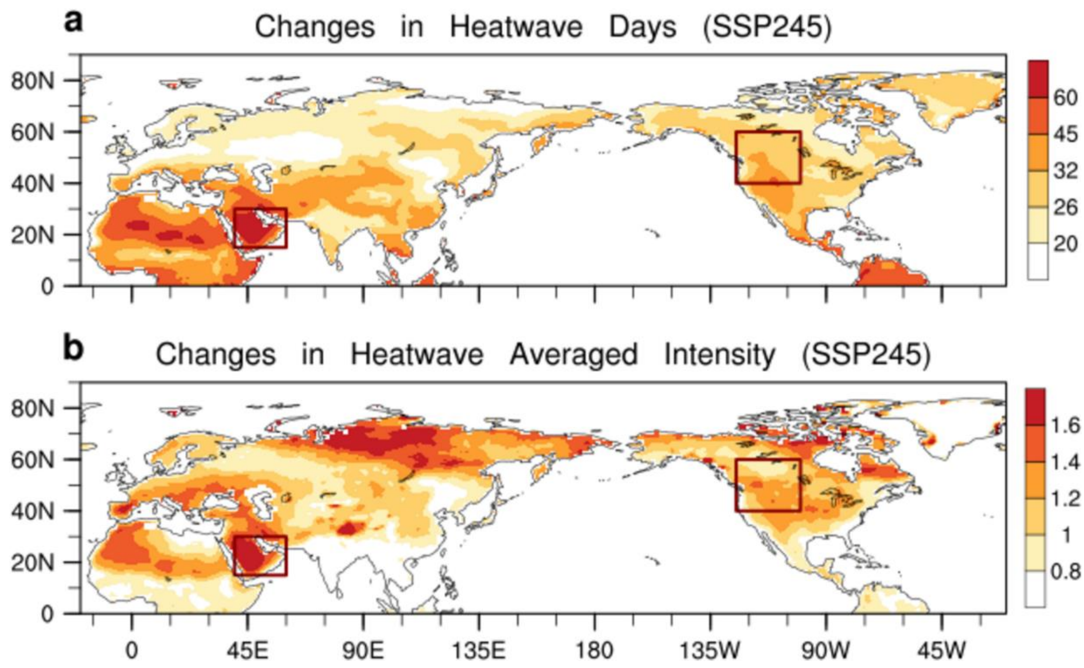

Figure S6. Multi-model mean of long-term future summertime heatwave changes in the Northern Hemisphere under the future SSP245 scenario. Same as Fig. S5, but for the SSP245 scenario.

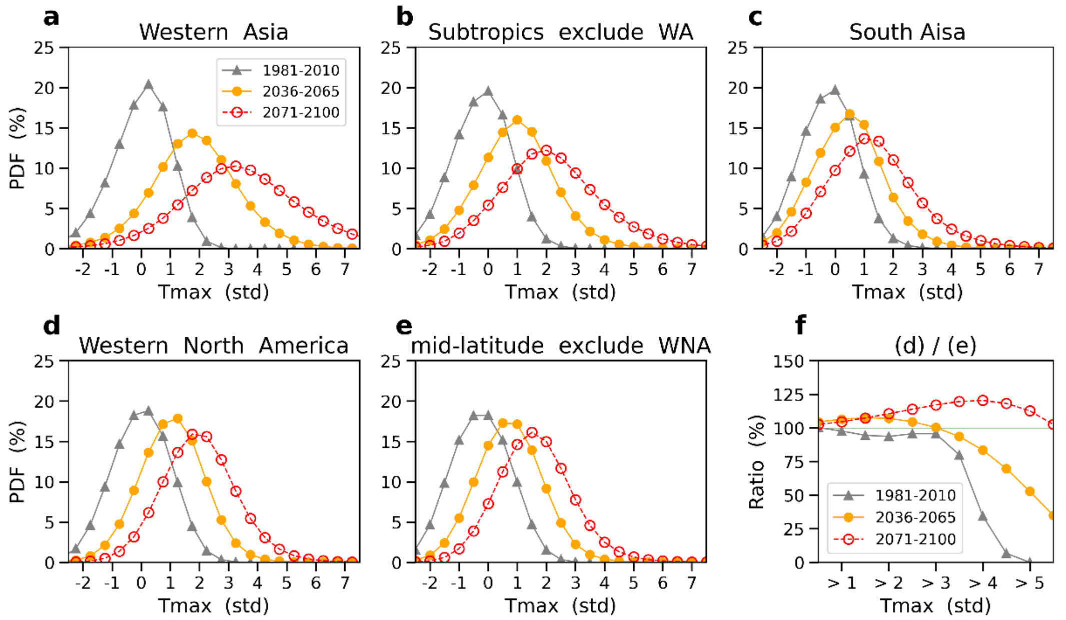

Figure S7. Projected probability density functions (PDF) of T_{max} over different regions. Probability density functions (PDF) of T_{max} over **(a)** western Asia (15°–30°N, 40°–60°E), **(b)** subtropical region (15°–30°N) excluding western Asia, **(c)** South Asia (15°–30°N, 70°–85°E), **(d)** western North America (40°–60°N, 125°–100°W), **(e)** mid-latitude region (40°–60°N) excluding western North America. **(f)** The ratio of accumulated PDF in T_{max} over western North America versus that over mid-latitude region (40°–60°N) excluding western North America.

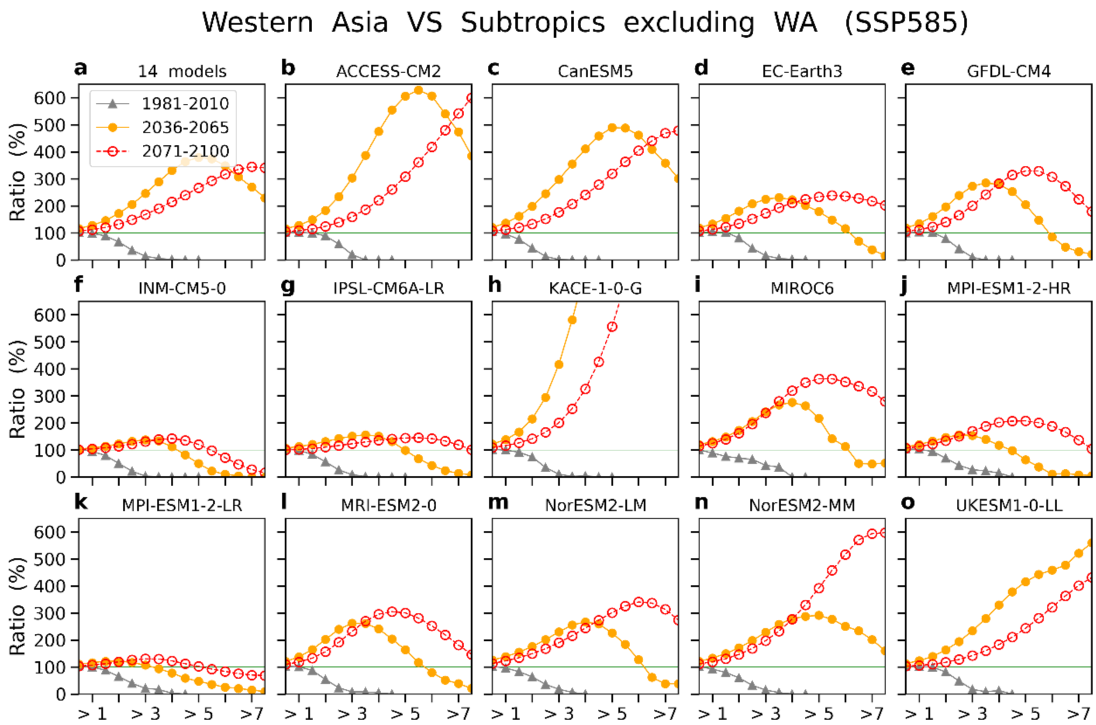

Figure S8. Accumulated probability density functions (PDF) of T_{max} over western Asia versus that over the subtropics. The ratio of accumulated PDF of T_{max} over western Asia versus that over subtropical region (15°–30°N) excluding western Asia simulated by models **(a)** ACCESS-CM2, **(b)** CanESM5, **(c)** EC-Earth3, **(d)** GFDL-CM4, **(e)** HadGEM3-GC31-LL, **(f)** INM-CM5-0, **(g)** IPSL-CM6A-LR, **(h)** MIROC6, **(i)** MPI-ESM1-2-HR, **(j)** MPI-ESM1-2-LR, **(k)** MRI-ESM2-0, **(l)** NorESM2-LM, **(m)** NorESM2-MM, and **(n)** UKESM1-0-LL. Results of PDF for the period 1981–2010 in historical simulation are shown by gray lines with triangles, and for the periods 2036–2065 and 2071–2100 under the SSP585 scenario by orange lines with solid circles and red lines with hollow circles, respectively.

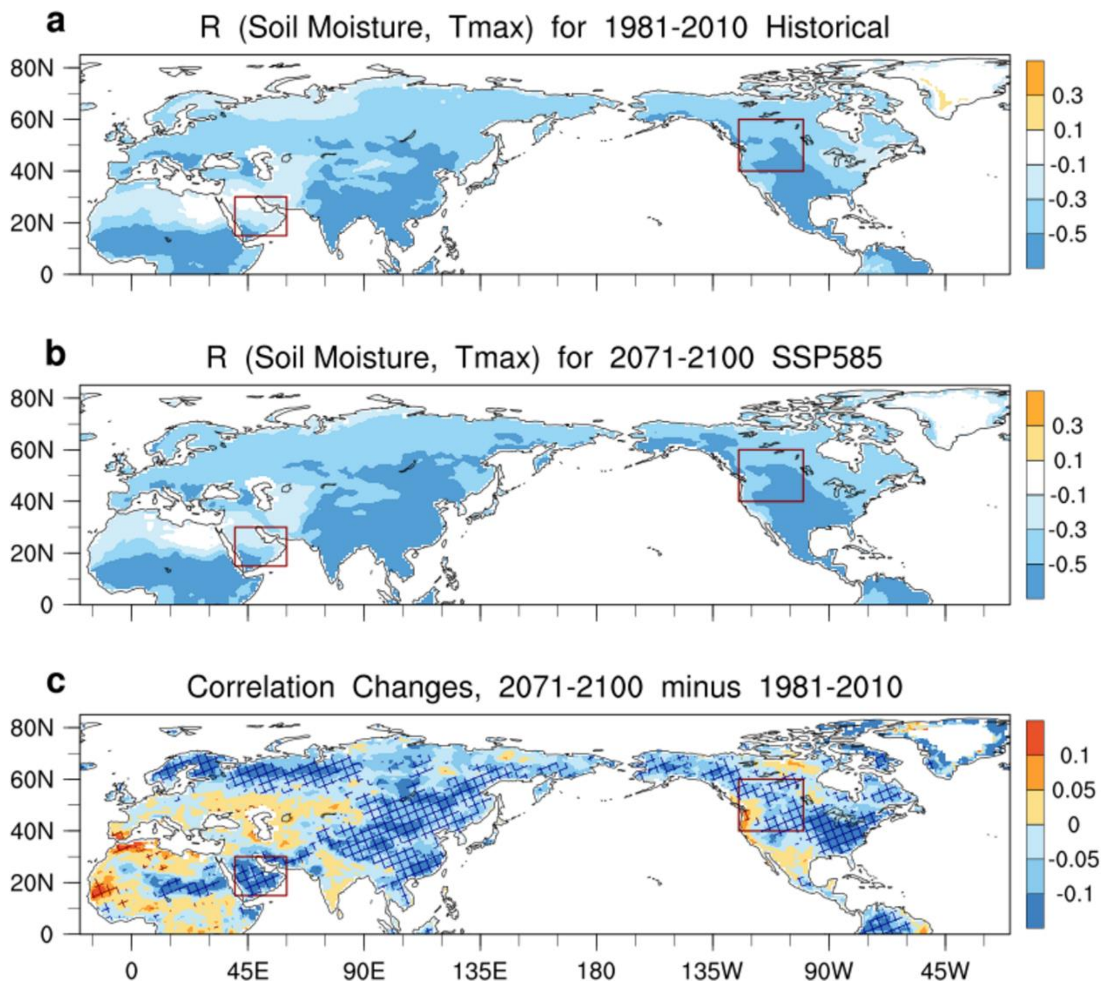

Figure S9. Multi-model median of daily correlations between soil moisture and T_{max} and its changes. Daily correlations between soil moisture and T_{max} for **(a)** the period 1981–2010 in historical simulations and **(b)** the period 2071–2100 under the SSP585 scenario, and **(c)** the difference between **(b)** and **(a)**. The spatial patterns in **(a–c)** are the median of results simulated by 14 CMIP6 models. Hatched areas in **(c)** show where at least 10 models (> 78% of the total 14 models) project the correlation changes with same signs.

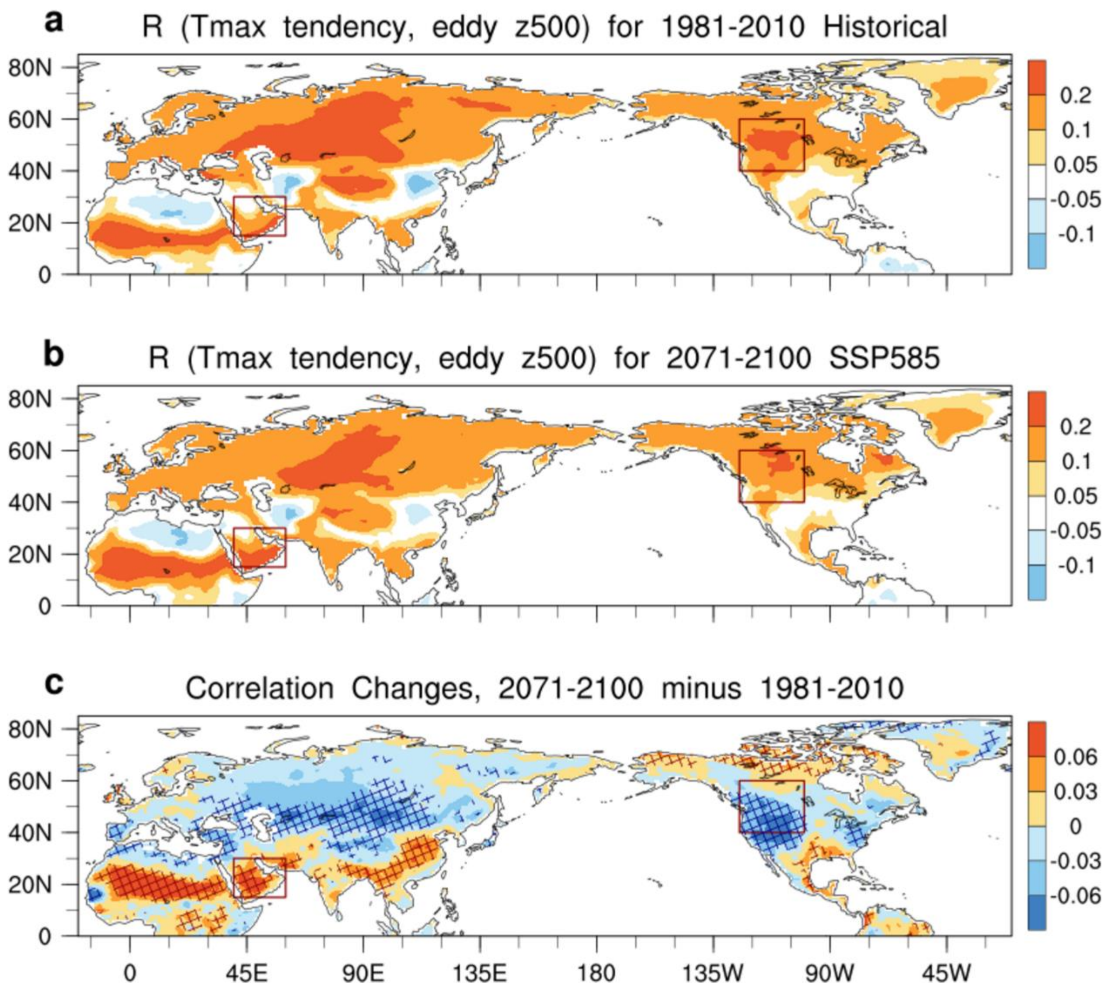

Figure S10. Multi-model median of daily correlations between soil moisture tendency and eddy z500 and its changes. Daily correlations between soil moisture tendency and eddy z500 for **(a)** the period 1981–2010 in historical simulations and **(b)** the period 2071–2100 under the SSP585 scenario, and **(c)** the difference between **(b)** and **(a)**. The spatial patterns in **(a–c)** are the median of results simulated by 14 CMIP6 models. Hatched areas in **(c)** show where at least 10 models (> 78% of the total 14 models) project the correlation changes with same signs.

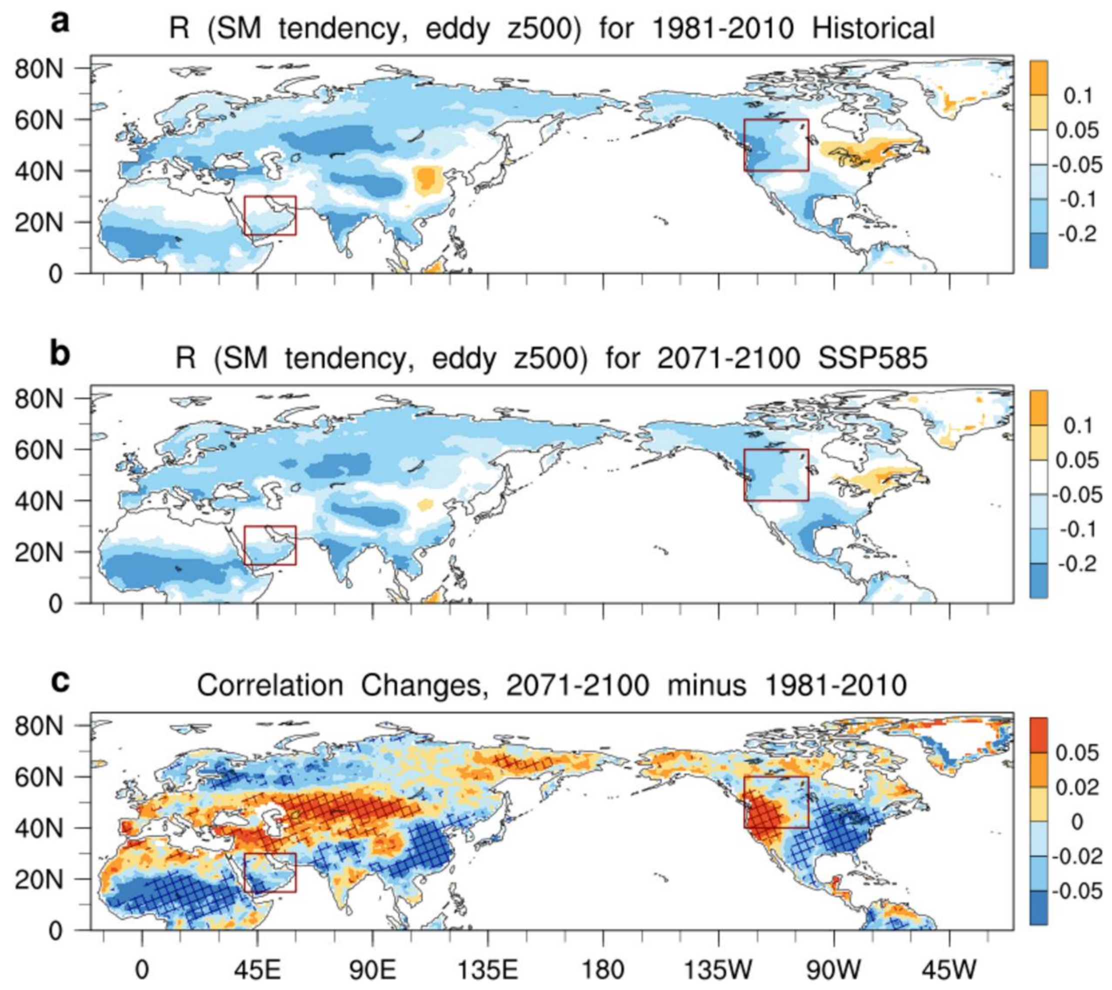

Figure S11. Multi-model median of daily correlations between T_{max} tendency and eddy z500 and its changes. Daily correlations between T_{max} tendency and eddy z500 for **(a)** the period 1981–2010 in historical simulations, **(b)** the period 2071–2100 under the SSP585 scenario, and **(c)** the difference between **(b)** and **(a)**. The spatial patterns in **(a–c)** are the median of results simulated by the 14 CMIP6 models. Hatched areas in **(c)** show where at least 10 models (> 78% of the total 14 models) project the correlation changes with same signs.